ChemPubSoc Europe

DOI: 10.1002/celc.201800848

CHEMELECTROCHEM Reviews

Special Collection

Electrochemical Impedance Spectroscopy Based Biosensors: Mechanistic Principles, Analytical Examples and Challenges towards Commercialization for Assays of Protein Cancer Biomarkers

Tomas Bertok,*[a] Lenka Lorencova,[a] Erika Chocholova,[a] Eduard Jane,[a] Alica Vikartovska,[a] Peter Kasak,[b] and Jan Tkac*[a]

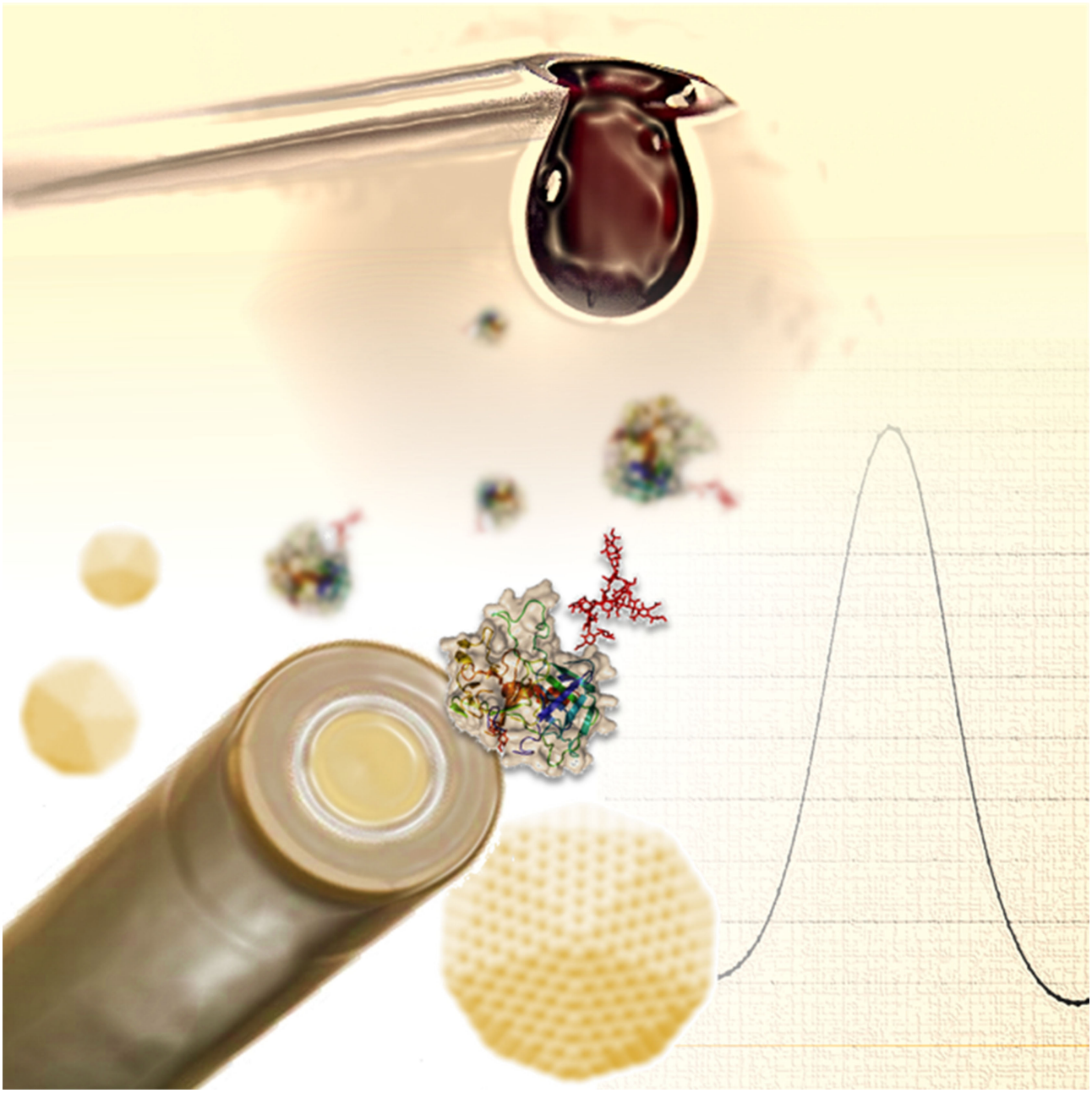

Impedimetric affinity biosensors are, without any doubt, among the most sensitive analytical devices available, offering low limits of detection and wide linear response ranges. There are, however, only a few papers detailing the application of impedimetric biosensors for the analysis of clinically relevant samples with due clinical performance. The fact that these devices have not found their way to any commercial or clinical use to date might be surprising, since an electrochemical assay platform based on portable potentiostats is a success story for monitoring a range of clinical parameters such as ions, haematological indicators and glucose. This review discusses the reasons behind this discrepancy and addresses the barriers to be overcome in order to achieve the point-of-care diagnostics using such devices for detection of protein oncomarkers approved by FDA. The final part of the review covers the most recent progress in the area.

1. Introduction

Portable electrochemical detection-based devices are common and have long been available with applications in environmental monitoring, the food industry[1–3] and also clinical diagnostics (e.g., Piccolo Xpress® or iStat handheld analyzers for measuring different ions or haematological parameters, such as haemoglobin, Hb).[4–6] Home glucose tests for monitoring diabetes are the most widely used,[7–9] despite the existence of similar devices for diabetics based on the MediSense®Optium™ platform.[10] The vast majority of biosensors (devices designed to detect or quantify a biomolecule) described in the literature to date involve enzyme-based biosensors (e.g., especially those based on glucose oxidase enzyme),[11] whilst immunosensors (antibody-based biosensors) are also fairly common.[12–15] These devices belong to a family of affinity biosensors which are based on a strong interaction between antibodies and analyte molecules from a clinical sample (e.g., blood, serum, urine, saliva, *etc.*).[12–14] Point-of-care diagnostics can benefit from this assay platform due to its various advantages, such as low assay cost and sample volume requirement, portability, moderate degree of multiplexing and, in special cases, also a label-free mode of operation.[16–19] Even though the U.S. biosensor market size was estimated to be 14.8 billion $ in 2015 (and is still growing, estimated to be 29 billion $ in 2024), impedimetric biosensors, although among the most sensitive, have not yet penetrated this market.[20,21]

Out of all the electroanalytical methods, electrochemical impedance spectroscopy (EIS) is one of the most complex, affording several advantages over the commonly used amperometry/potentiometry (e.g., wide linear range, low limit of detection (LOD) and label-free mode of operation).[22] To overcome the drawbacks of traditional laboratory electrochemical instrumentations, complementary metal oxide semiconductor instrumentation circuits have been reported and recently summarized.[23] Very often, EIS is combined with different nanostructured interfaces in order to increase the amount of biorecognition elements on the surface, and, hence, to enhance the performance of the biosensor in terms of assay sensitivity and extension of linear range. Functionalized carbon nanomaterials (or even modified screen-printed electrodes, SPE), such as graphene or boron-doped diamond, are currently commonly used and commercially available for the immobilization of biomolecules.[24–26] There exists, however, the prerequisite that the stability of the SPE reference electrode is crucial for the robustness of disposable impedimetric biosensors. The reference electrode should ideally be non-polarizable, e.g., must provide high-exchange current densities, and thus should not cause any potential drifts during storage and operation.[27,28]

This review focuses on the main principles and applications of EIS and on the challenges to be overcome in order to commercialize impedimetric biosensors for clinical diagnostics.[29] Herein, only those papers related to detection of protein biomarkers approved by the FDA (US Food and Drug Administration) are discussed and the reader is advised to read the excellent review papers in the event of interest in the electrochemical/impedimetric detection of genetic biomarkers like DNA, mRNA and miRNA for diagnostic purposes.[30–32] A section on different circuit models for fitting, experimental data evaluation and interpretation is also included, since this is frequently the main source of errors and misunderstandings in impedimetric measurements. Other problems, such as non-specific interactions of high-abundant interferents in biological matrices and reproducible, high-throughput analyses in an array format of analysis are also discussed.

2. Theoretical Background of Impedance Spectroscopy

(Operational) impedance is generally defined in accordance with Eq. (1):

$$\hat{Z}(s) = \frac{L[e(t)]}{L[I(t)]} = \frac{\bar{E}(s)}{\bar{I}(s)} \quad (1)$$

where L denotes Laplace transform, E and I denote the potential and current, respectively, and the parameter s (in classical Laplace transform expression is real, $s=\sigma$, though it

[a] Dr. T. Bertok, Dr. L. Lorencova, E. Chocholova, Dr. E. Jane, Dr. A. Vikartovska, Dr. J. Tkac
Department of Glycobiotechnology
Institution of Chemistry
Slovak Academy of Sciences
Dubravska cesta 9, 845 38 Bratislava, Slovakia
E-mail: Tomas.Bertok@savba.sk
Jan.Tkac@savba.sk
[b] Dr. P. Kasak
Center for Advanced Materials
Qatar University
Doha 2713, Qatar
An invited contribution to a Special Collection dedicated to Bioelectrochemistry

might also be complex, $s=\sigma+j\omega$) is denoted as the frequency. This is generally valid for any potential perturbation; however, in electrochemical impedance spectroscopy, an AC signal stimulus is usually applied, hence the following Fourier transform [Eq. (2)] is applied for sinusoidal perturbation:

$$\hat{Z}(j\omega)=\frac{F[E(t)]}{F[I(t)]}=\frac{\tilde{E}(j\omega)}{\tilde{I}(j\omega)}=Z_{REAL}(\omega)+jZ_{IMAG}(\omega) \quad (2)$$

where for the so-called AC impedance, the parameter s is an imaginary one, i.e., $s=j\omega$ ($j=\sqrt{-1}$), Z_{REAL} and Z_{IMAG} are the real and imaginary parts of the impedance, respectively. Besides impedance, admittance (inverse expression of impedance, Y) is a frequently used term, and impedance and admittance together are denoted as immittances.[33,34] Electrical circuits contain three passive elements, namely resistors, capacitors and inductors. For AC impedance, mainly resistors (R) and capacitors (C) are considered. For linear electrical elements R and C, the AC impedance of these elements is R and $1/j\omega C$, respectively. The impedance of the total circuit with different elements in series/parallel connection is then written using Ohm's and Kirchoff's laws. The linear part (at lower frequencies) is only of any physical significance in Faradaic EIS and represents the delay arising from diffusion of electroactive species to the electrode.[35]

However, various possible mechanisms for impedance change upon the binding target analyte should be discussed. The plot of the imaginary *vs.* real part of Z [as in Eq. (2)], the so-called Nyquist plot (Figure 1, more correctly an Argand diagram), is subsequently evaluated and fitted using a model circuit to obtain the characteristics of the system under study, such as double-layer capacitance (the sum of a constant capacitance of an unmodified electrode and a variable capacitance originating from a surface modifier) or electrolyte/charge transfer (i.e., the sum of an unmodified electrode and an introduced modifier) resistance.[32] For rough surfaces, the

Dr. Tomas Bertok gained his PhD degree at the Department of Biochemical Technology, Slovak University of Technology in Bratislava. He is an independent research scientist at the Institute of Chemistry at the Slovak Academy of Sciences, a supervisor for PhD study in biochemistry and biotechnology and former Scientist of the Year under 35 for Slovakia (2016). He is currently working in the area of novel diagnostic devices and assays development using nanomaterials.

Dr. Lenka Lorencova obtained her PhD degree at the Department of Biochemistry at Comenius University in Bratislava, Slovakia. She currently works as a research scientist at the Institute of Chemistry, Slovak Academy of Sciences in Bratislava. Her research interests include advanced electrochemical characterization techniques, design of electrochemical biosensors, surface science and nanotechnology.

Erika Chocholova obtained her Master's degree in biochemistry in 2015 at Comenius University, Faculty of Natural Sciences in Bratislava. Currently, she is a PhD student at the Slovak University of Technology. She works at the Department of Glycobiotechnology, Institute of Chemistry, Slovak Academy of Sciences under the guidance of Tomas Bertok. Her research focuses on electrochemical biosensors and surface modification for medical purposes using nanotechnology.

Dr. Eduard Jane gained his PhD in physical chemistry in 2014 at Comenius University in Bratislava. He is currently working as a research assistant at the Institute of Chemistry at the Slovak Academy of Sciences in Bratislava. His research interests are mass spectrometry combined with other separation and sample pre-treatment techniques, biosensors, machine-learning algorithms and nanotechnology.

Dr. Alica Vikartovska gained her PhD degree in biochemistry at the Institute of Chemistry, Slovak Academy of Sciences in 1998. Since 1990 she has worked at the Department of Glycobiotechnology, Institute of Chemistry at the Slovak Academy of Sciences. Her research interests are: the immobilization of enzymes and cells, enzyme kinetics, and the characterization of immobilized biocatalysts using thermal biosensor (enzyme thermistor) and glycomics.

Dr. Peter Kasak worked in the group of Professor R. J. M. Nolte at Radboud University, Nijmegen in 2001. In 2004 he obtained a Lisa Meitner postdoctoral fellowship at the University of Vienna before starting research at the Polymer Institute, Slovak Academy of Sciences, where he was a senior researcher. From 2012, he has worked in the Centre for Advanced Materials at Qatar University. His research interests include catalysis, modification of surfaces, development of biocompatible hydrogel matrices, and study of the mechanism of free radical polymerization.

Dr. Jan Tkac is Head of the Department of Glycobiotechnology at the Institute of Chemistry, Slovak Academy of Sciences. He studied as a postdoc at Linkopings Universitet, Lunds Universitet and Oxford University. His research activities cover label-free and label-based platforms of detection, nanoscale surface patterning protocols, catalytic biosensors and biofuel cells, glycan biochips/biosensors, and lectin/antibody-based-affinity biosensors/biochips. In the past, he was the recipient of an Individual Marie Curie Fellowship, ERC Consolidator grant and currently ERC Proof of Concept grant.

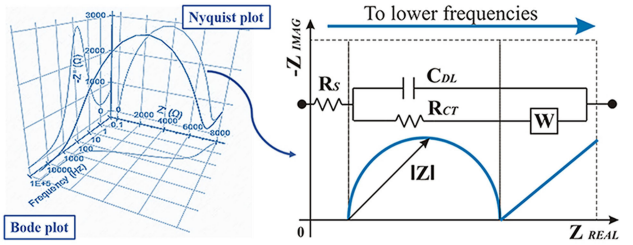

Figure 1. Complex plane Nyquist and Bode diagrams as projections within a 3D diagram (left). Two parameters i.e., double layer capacitance and charge transfer resistance (semicircle diameter, R_{CT}) are extracted from the Nyquist plot (right). The R_{CT} value (shown in detail on the right) tends to increase after a biorecognition event takes place, but other issues may significantly affect the R_{CT}, such as electrostatic attraction/repulsion between a charged layer (proteins, DNA, *etc.*) and a charged mediator.

electronic properties of the interface cannot be adequately described with a capacitive element, hence a constant phase element (CPE) is used instead. Solid electrodes are not ideally polarizable (compared to liquid ones like mercury), so they usually do not retain a purely capacitive electrochemical double-layer. The lack of homogeneity during impedance studies is modelled with CPE, represented by the Q symbol in the Randles-Erschler equivalent circuit, e.g., R(Q[RW]). The impedance of CPE is described in Eq. (3) as:

$$Z_Q = {}^{1}/_{Y_0(j\omega)^n} \quad (3)$$

where n is an empirical constant. When n approaches 1, the CPE acts as an ideal capacitor and, by contrast, when $n = 0$, it becomes a pure resistor.[36] For impedimetric biosensors, Faradaic EIS is most commonly used, i.e., using an electrochemical mediator dissolved in a working electrolyte, such as a ferri/ferrocyanide redox couple.

However, when Faradaic EIS using a ferri/ferrocyanide redox couple is combined with Au electrodes, the Au surface is seriously damaged over time by Au atoms, which are etched by CN^- ions and the process could not be completely suppressed even under optimal conditions.[37] Hence, even though self-assembled monolayers (SAMs) on Au electrodes offer several advantages, such as possibility to control the surface density and orientation of biorecognition elements, suppression of the non-specific interactions (an issue addressed below), the ability to tune initial R_{CT} during an experiment (by properly chosen terminal SAM functionalities) compared to other types of electrodes,[38,39] the repeated or long-term use of such an Au modified electrode should be avoided when using a Faradaic EIS detection scheme.

3. Circuit Modelling, Data Interpretation and Validation

Biorecognition events on the biosensor surface are usually manifested as a phase and an amplitude shift in the response relative to the stimulus signal, and typically modelled using a Randles circuit (proposed by John Edward Brough Randles).[23,40] However, accurate data interpretation might be difficult when non-ideal Nyquist plots are obtained during an experiment (caused by non-homogenous surface modification, interface defects, *etc.*), such as two and more semi-circular regions. Typical forms of a Nyquist diagram for different circuits are shown in Figure 2. However, more complex, less ideal forms of the plots may occur during a measurement.

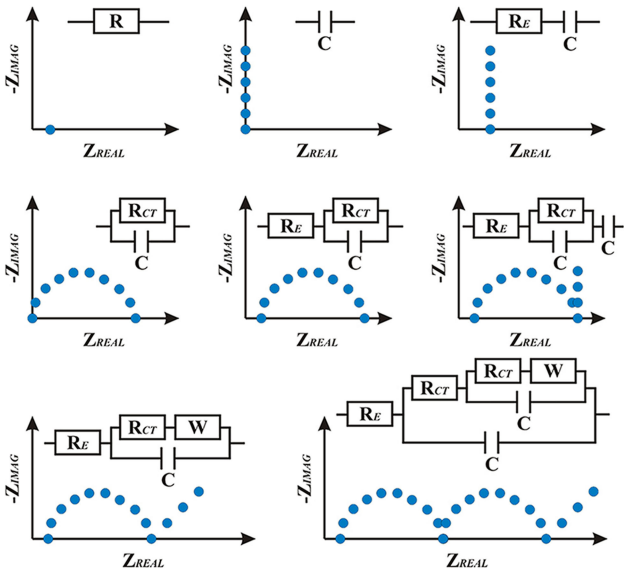

Figure 2. Typical Nyquist plots for various electrical circuits, moving from those that are the most simple to the most common. **Upper row** (from left to right): pure resistor (R, only real part of impedance); pure capacitor (C, only imaginary part of impedance); R and C in series connection. **Middle row** (from left to right): R and C in parallel connection; R and C in parallel connection with an electrolyte resistance (R_E) – where R_{CT} denotes the charge (or electron) transfer resistance of the interface; the same circuit with additional capacitance in series. **Lower row left**: Randles-Ershler equivalent circuit, most commonly used for fitting impedimetric biosensor data, where W stands for Warburg element (diffusion parameter for low frequencies). **Lower row right**: more complex system with two semicircular regions, i.e., two interfacial charge transfer resistances. Reprinted from,[53] Copyright 2014 with permission from Elsevier.

Especially for biological interactions, these facts must be carefully evaluated and require proper interpretation, which can be a substantial impediment in the development of any "user-friendly" portable device operated by a non-specialist (e.g., a patient). The main reason is that impedimetric assays do not permit a simple "click-and-go" measurement method in most cases. Another challenge for point-of-care impedimetric devices is assay selectivity for clinical applications, since whole blood or serum contains a significant amount of non-target molecules, which can be more abundant than the biomarker of interest. Even though the impedimetric biosensors often afford low LOD (down to fM/aM level)[41–43] and a wide linear response range,[44,45] in many cases analyte pre-separation as well as a nanoscale controlled surface chemistry need to be applied in order to achieve biomarker detection without using additional labels.

For instance, the prostate specific antigen (PSA, a prostate cancer biomarker) needs to be selectively detected at concentrations of several ng mL^{-1}. Currently, more than 4.0 ng mL^{-1} PSA level in blood is deemed to be pathological and further examinations (often a biopsy) are needed to exclude other non-malignant processes, such as benign prostate hyperplasia, and to confirm prostate cancer.[46,47] For example, the application of a biosensor for PSA detection in human serum without any additional separation steps would be useless if a biosensor would non-specifically bind human serum albumin, which is present at a concentration 6 orders of magnitude higher (up to 50 mg mL^{-1}) than PSA. Controlled sample delivery to the device interface is also an important additional step, since manual sample delivery without any (micro)fluidics may lead to significant errors affecting the device performance and clinical outcome of such assays.

Frequency Response Analyzers (FRA modules) are commonly a part of laboratory potentiostats/galvanostats and might also be a part of some portable devices (i.e., for PalmSens or Ivium Technologies).[48,49] They are not intended for diagnostic purposes, however. For these kinds of devices, there is often a problem with shielding, since three main conditions must be met for every impedimetric measurement: linearity (the AC amplitude needs to be small enough to keep the response linear, but at the same time high enough to increase the signal-to-noise ratio), stability (the system cannot change during measurement i.e., data acquisition) and causality (the AC response needs to correlate with the AC stimulus only, i.e., shielding is an important feature, for example, for the small currents obtained during potentiostatic EIS).[50] These three conditions might be difficult to achieve in home diagnostic devices, which is another important issue that needs to be overcome for the commercial success of the impedimetric biosensor design. Even though potentiostatic impedance measurements are often performed using a wide range of different frequencies, it is possible to measure the impedance in real time at a single frequency or to perform assays using devices with integrated microfluidics.[35,51] Once the data are acquired, appropriate interpretation is crucial. This is often a difficult task, even for a skilled scientist, since more than one single-circuit model can actually meet the requirement to obtain a statistically significant fitting.[52] It is a general rule that the papers dealing with impedimetric biosensors usually use the Randles equivalent circuit to obtain the R_{CT} value as an output signal. However, there are some papers dealing with the "two semicircles" problem, although the vast majority do not describe the application of biosensors.

Ohno *et al.* suggested that, for an IgA biosensor device, the organic layer-modified electrode surface was actually divided into two parts: an interfacial part (expressed as a parallel connection of R_{CT} and C_{DL}) and an inner part (expressed as constant R and CPE). After binding of the IgA sample to the anti-IgA layer, only R_{CT} increased, and LOD of 0.01 ng mL^{-1} could be achieved.[54]

Other examples of using circuit models other than the Randles circuit R(C[RW]) for Nyquist plots with two visible semicircular regions have also been described, e.g., immunosensors for the detection of ciprofloxacin antibiotic (using R(RC)(RC) circuit with LOD of 10 pg mL^{-1})[55], biosensors using R(RC)(C(RW)) circuit for assay of interleukin-6 (with LOD of 10 ag mL^{-1}) or 1,10-phenanthroline-5,6-dione- and glucose oxidase-modified graphite electrode[56,57] and even for the analysis of whole HeLa cells (for cervical cancer diagnostics) using R(C(R(RC))) circuit with LOD of 10 cells mL^{-1}.[58]

For non-Faradaic EIS measurements, Cole-Cole complex capacitance plots ($-C_{IMAG}$ *vs.* C_{REAL}) are sometimes constructed from data obtained during an experiment using the following equation [(Eq. (4)][59]:

$$C^* = C^{I} + jC^{II} = \frac{1}{j\omega Z} = \frac{-Z^{II}}{j\omega|Z|^2} \quad (4)$$

Davis's group published a series of papers on impedance-derived capacitance spectroscopy and its diagnostic utility (for detection of prostatic acid phosphatase down to 11 pM and C-reactive protein down to 28 pM).[60,61]

EIS affords a major advantage over other electroanalytical methods i.e., validation of experimentally obtained data using a Kramers-Kronig (KK) test. The KK relations are mathematical expressions connecting the experimentally obtained imaginary/real part of the impedance (or a complex function, in general) with its real/imaginary counterpart. The experimental data are fitted using a circuit which always satisfies KK relations, so the KK transform (in combination with other methods) acts as an independent check against invalid experimental data.[35,50,62,63] This approach should always be applied to EIS assays and was used, for example, for the validation of disposable biosensor assays using a single-frequency impedance detecting haptoglobin (Hp)[64] or HSP70 (heat shock protein 70, a tumor biomarker) by the same SFI method down to 12 fg mL^{-1} [65].

Besides Nyquist ($-Z_{IMAG}$ *vs.* Z_{REAL}) and Bode (modulus [Ω] / phase [°] *vs.* frequency [Hz]) plots, two other types of plots may serve as a validation tool for each point during EIS measurements in real time. The first one is a Lissajou plot (AC current *vs.* AC potential), which exhibits a central symmetry with regard to the origin of the plot, when the linearity condition is fulfilled. The second one is a Resolution plot (AC current and AC potential *vs.* time), which indicates whether the sensitivity of the system is sufficient and the noise is kept to a minimal value.[66]

There are several free and commercially available software packages for data evaluation and fitting (such as LEVM and EIS spectrum analyzer or ZView and ZSimpWin, respectively)[35], and all the methods previously described are commonly integrated within the software that comes with the commercial potentiostats/galvanostats, such as NOVA software (Metrohm) or PSTrace (PalmSens). Each potentially commercialized impedimetric biosensor needs to come with software for such data validation in order to provide a user-friendly interface since, due to the complexity of EIS measurements, it is impossible to make such devices as simple as current glucose biosensors, which essentially are a "black box" for the user, not needing any strategic intervention/decision.

Another option for interpreting EIS spectra is based on the analysis of Poisson-Nernst-Planck equations (PNP).[67–69] The simplest case of PNP assumes the presence of only positive and negative ions in the solution. For simplicity, only a one-dimensional case is described. The sample solution is placed between the electrodes sited at positions 0 and *d*. A simplified geometry of the system is shown in Figure 3. The recombination and further reaction of ions in solution for simplicity is excluded. The external perturbation of an electrical field is small, so only local oscillation in the concentration is assumed [Eq. (5)].[70]

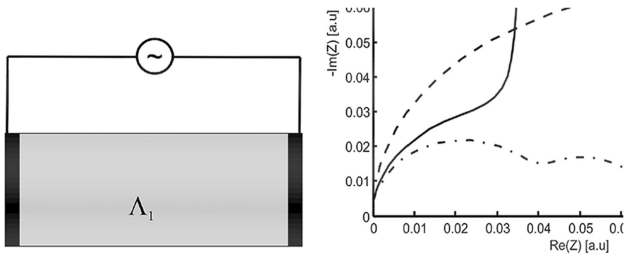

Figure 3. Nyquist plot for different boundary conditions (solid: blocking; dashed: Chang-Jaffe; dash-dotted: Ohmic boundaries).

$$c_i = c_0 + c_{i1}\exp(i\omega t), \quad i = cation/anion \tag{5}$$

where c_i is the bulk concentration and c_{i1} is the local concentration of ion. The c_0 is thermodynamically bulk ion concentration. The electrodes are perpendicular to the z axis. Once these assumptions are taken into account, the governing equations for the electric field are described in the Poisson equation [Eq. (6)],[71]

$$\frac{\partial^2 V}{\partial z^2} = -\frac{q}{\varepsilon}(c_{11} - c_{21}) \tag{6}$$

and the conservation law for the ions [Eq. (7)] as:

$$\frac{\partial c_{i1}}{\partial t} = D\frac{\partial}{\partial z}\left\{\frac{\partial c_{i1}}{\partial z} \pm \frac{q}{K_B T}(c_0 + c_{i1})\frac{\partial V}{\partial z}\right\} \tag{7}$$

where ε is the permittivity of the liquid, q is the elementary charge, K_B is the Boltzman constant, D is the diffusion coefficient (assuming that the cations and anions have an equal value of D), z is the spatial coordination. Note that all concentrations are spatial and time-resolved: $c_0 = c_0(z,t)$, $c_{i1} = c_{i1}(z,t)$, $V = V(z,t)$. The boundary condition for the electric field [Eq. (8)] is:

$$V(z_0, t) = \pm\frac{V_{max}}{2}\exp(-i\omega t) \tag{8}$$

The boundary conditions for the ions are[72]:

A) Blocking boundary conditions. The ion current for cations and anions is 0 [Eq. (9)]:

$$\frac{\partial c_{i1}(z_0,t)}{\partial z} \pm \frac{q}{K_B T}(c_0(z_0,t) + c_{i1}(z_0,t))\frac{\partial V(z_0,t)}{\partial z} = 0; \quad z_0 = 0, d \tag{9}$$

B) Chang-Jaffe boundary conditions. The ion current is proportional to the concentration of ions [Eq. (10)]:

$$\frac{\partial c_{i1}(z_0,t)}{\partial z} \pm \frac{q}{K_B T}(c_0(z_0,t) + c_{i1}(z_0,t))\frac{\partial V(z_0,t)}{\partial z} = k c_{i1}(z_0 t) \quad z_0 = 0, d \tag{10}$$

C) Ohmic boundary. The ion current is proportional to the surface electric field [Eq. (11)]:

$$\frac{\partial c_{i1}(z_0,t)}{\partial z} \pm \frac{q}{K_B T}(c_0(z_0,t) + c_{i1}(z_0,t))\frac{\partial V(z_0,t)}{\partial z} = \sigma V(z_0 t) \quad z_0 = 0, d \tag{11}$$

After the Laplace transformation, the partial differential equations are reduced to ordinary differential equations. Some useful substitutions are necessary to solve these equations.[73] These substitutions can be summarized as follows [Eq. (12)]:

$$Z = \frac{z}{d}; \quad \tau = D\frac{t}{d\lambda_D}; \quad \varphi = \frac{q}{K_B T}V; \quad C_i = \frac{c_{i1}}{c_0}; \quad \lambda_D = \sqrt{\frac{\in K_B T}{2e^2 c_0}} \quad \Lambda = \frac{\lambda_D}{d} \tag{12}$$

where Z is the dimensionless coordinate, d is the length between the electrodes, τ is the dimensionless time, capital C is the dimensionless concentration and λ_d is the Debye length. The governing equation can then be expressed as [Eq. (13), (14)]:

$$\Lambda^2\frac{\partial^2\varphi}{\partial Z^2} = -c_0(C_{11} - C_{21}) \tag{13}$$

$$\frac{\partial c_{i1}}{\partial \tau} = \Lambda c_0\frac{\partial}{\partial Z}\left(\frac{\partial c_{i1}}{\partial Z} + (1 + C_{i1})\frac{\partial\varphi}{\partial Z}\right) \tag{14}$$

The NP equation is Laplace transformed to [Eq. (15)]:

$$i\omega C_{i1} = \Lambda c_0\frac{\partial}{\partial Z}\left(\frac{\partial c_{i1}}{\partial Z} + (1 + C_{i1})\frac{\partial\varphi}{\partial Z}\right) \tag{15}$$

Note that now all C, φ are frequency- and spatial-coordinate- dependent.

The numerical result of this equation is shown in Figure 3. The blocking boundary conditions have a Nyquist plot similar to the equivalent circuit shown in Figure 2. The Ohmic boundary has a Nyquist plot similar to a circuit with 2 resistances.

Following the assumption that the bulk concentration c_0 is much larger than c_{i1}, $c_0 \gg c_{i1}$ this model has an analytical solution and can serve as a benchmark for the numerical computations.[72] The application of PNP with slight modifications is used for Li-batteries simulation,[74,75] transport,[76] biosensors,[77] *etc.*

One of the modifications of the PNP system was used to simulate ionic polymer composites (IPMC). This two-layer system consists of IPMC and a polymer membrane. In the

composite layer, free electrons can migrate and the total current generated is the sum of the migrating ions and electrons. This system can be simulated with an equivalent circuit, consisting of resistance, capacitance and Warburg impedance element in parallel.[78] A further implementation of the PNP system was to model a zwitterionic hydrogel layer. The zwitterionic hydrogel layer contains four different ions i.e., H^+ and OH^- ions from the hydrogel and cations and anions from the electrolyte solution. Moreover, an equilibrium pertains between the H^+ and OH^- ions governed by the dissociation constant at a particular pH of the electrolyte. The result from the simulations was that the hydrogel resistance and double-layer capacitance depend on the pH value.[70]The simulations in the area of biosensors are based on the assumption that a large biomolecule has a dielectric constant very different from that of the electrolyte.[79] Hence, in this case, the biomolecule has a different capacitance and resistance. In the dimensional case, the biomolecule is simulated as a layer with parameters different from the bulk electrolyte. This basic one-dimensional model with Nyquist plots for various Λ_2 positions is shown in Figure 4.[80] The models were applied to simulations on the

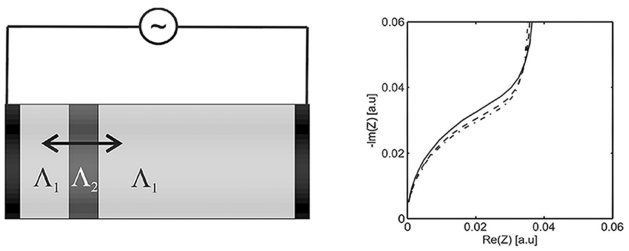

Figure 4. Nyquist plot for different position of layer. Solid line is the nearest to the electrode, dash-dotted is the furthest.

nanoelectrodes set in the array format. There are attempts to model the interfacial biosensor's interfaces in two/three spatial dimensions. The impedimetric biosensor with a passivation layer was subsequently used for detecting pathogen bacterial cells.[81]

4. EIS as a Powerful Tool for Sensitive Detection of Cancer Biomarkers

The phrase "tumor marker" is often transposed for the term "biomarker" and *vice versa*. According to the National Institutes of Health, a biomarker is defined as a cellular, biochemical and/or molecular characteristic that can be objectively measured and evaluated as an indicator of normal biological processes, pathological processes or pharmacological responses to therapeutic intervention.[82] In contrast, the definition of a tumor marker is more specific. A tumor or cancer marker may be defined as a substance produced by a tumor or by the host in response to a cancer cell that can be objectively measured and evaluated as an indicator of cancerous processes within the body.[83] To date, the U.S. Food and Drug Administration (FDA) has approved 19 protein cancer markers, 11 present in blood, 5 detectable in tissue and 3 located in urine (Table 1).[84] Although various methods were tested for the evaluation of these markers, there are just a few markers which were detected by the EIS-based biosensors.

Table 1. List of FDA-approved protein cancer biomarkers.[84]

Biomarker	Sample	Use	Cancer	Assay
AFP	S	St	TeCa	IA
β-hGC	S	St	TeCa	IA
CA 19–9	S	Mo	PaCa	IA
CA 125	S	Mo	OvCa	IA
CA 15.3	S	Mo	BCa	IA
CA 27.29	S	Mo	BCa	IA
CEA	S	Mo	CCa	IA
FDP	S	Mo	BlCa	IA
HE4	S	Mo	OvCa	IA
PSA	S	Sc& Mo	PCa	IA
TG	S	Mo	TCa	IA
EGFR	T	Pre	CCa	IHC
KIT	T	Pre	GaCa	IHC
ER	T	Pre & Pro	BCa	IHC
PR	T	Pre & Pro	BCa	IHC
HER2-neu	T	Pre & Pro	BCa	IHC
NMP/22	U	Sc& Mo	BlCa	IA
BTA	U	Mo	BlCa	IA
↑ Mw CEA	U	Mo	BlCa	IF

Abbreviations: AFP: α-fetoprotein; β-hGC: human chorionic gonadotropin-β; CA 19–9: carbohydrate antigen 19–9; CA 125: carbohydrate antigen 125; CA 15.3: carbohydrate antigen 15.3; CA 27.29: carbohydrate antigen 27.29; CEA: carcinoembryonic antigen; FDP: fibrin/fibrinogen degradation products; HE4: human epididymis protein 4; PSA: prostate specific antigen; TG: thyroglobulin; EGFR: pidermal growth factor receptor; KIT: v-kit Hardy-Zuckerman 4 feline sarcoma viral oncogene homolog; ER: estrogen receptor; PR: progesterone receptor; HER2-neu: human epidermal growth factor receptor 2; NMP/22: nuclear matrix protein 22; BTA: bladder tumour antigen; ↑ Mw CEA: high molecular mass CEA; S: serum; U: urine; T: tissue; St: staging; Mo: monitoring; Sc: screening; Pre: predictions; Pro: prognosis; TeCa: testicular cancer; PaCa: pancreatic cancer; OvCa: ovarian cancer; BCa: breast cancer; CCa: colorectal cancer; BlCa: bladder cancer; PCa: prostate cancer; TCa: thyroid cancer; GaCa: gastrointestinal cancer; IA: immunoassays; IHC: immunohistochemistry; IF: immunofluorescence.

4.1. α-Fetoprotein

α-Fetoprotein (AFP) is a serum protein with a molecular mass of 70 kDa, which is produced by the yolk sac and the liver during fetal life. Normally, the level of AFP in the serum of healthy human individuals is under 25 ng mL^{-1}, but this value rises with the development of some cancerous diseases (hepatocellular cancer, yolk sac cancer, liver metastasis from gastric cancer, testicular cancer, and nasopharyngeal cancer). Accordingly, it is one of the most extensively used clinical cancer biomarkers.[85]

In 2013, Zhang and co-workers developed a sensitive label-free electrochemical EIS biosensor array based on five screen-printed carbon electrodes (SPCE) covered with carboxyl-functionalized single-wall carbon nanotubes (SWNTs) for the detection of AFP.[86] Molecules of wheat-germ agglutinin (WGA) lectin were immobilized on the SWNTs layer and served as a

specific recognition element. The biosensor had a linear response range from 1 to 100 ng L^{-1} with LOD of 0.1 ng L^{-1}. In addition, thanks to a lectin-based biosensor array prepared with five different lectins, it was possible to discriminate between healthy and cancer patients serum samples based on different glycan compositions in AFP protein.[86]

Yuan with his team just a year later showed the integration of nanomaterials into an EIS assay format for the detection of AFP.[87] They prepared a sandwich-type EIS immunosensor (Figure 5). The biosensor was built on a glassy carbon electrode

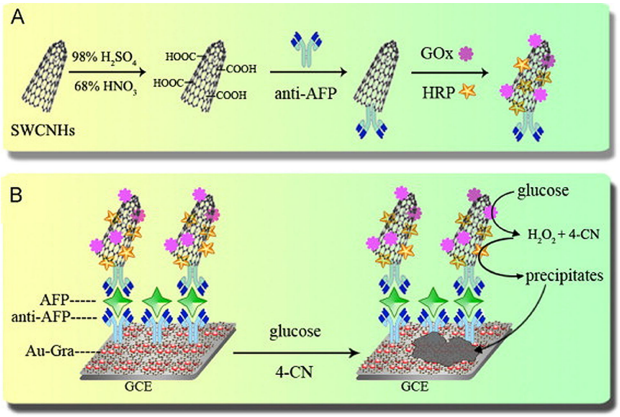

Figure 5. Preparation of SWCNHs-bienzymatic-Anti2-AFP bioconjugates using carboxy-groups on surface (A) and stepwise functionality of a modified electrode (B), where GCE is modified by Au-Gra layer and subsequently with anti-AFP antibody. AFP is detected in a sandwich configuration. Reprinted from [87], Copyright 2014 with permission from Elsevier.

(GCE) modified with gold nanoparticles/graphene nanosheet nanocomposites (Au-Gra), which served as a matrix for the attachment of primary antibodies (Anti1-AFP). The second step was the application of a complex consisting of secondary antibodies (Anti2-AFP) and two enzymes (horseradish peroxidase-HRP and glucose oxidase-GOx) attached to the surface of functionalized single-walled carbon nanohorns (SWCNHs). The biocatalyst accelerated the oxidation of 4-chloro-1-naphthol (4-CN) by H_2O_2 to yield an insoluble product on the electrode, which blocked the interfacial electron transfer of a redox probe and thus enhanced detection sensitivity. The immunosensor showed a wide dynamic range between 1 pg mL^{-1} and 60 ng mL^{-1} with LOD of 0.33 pg mL^{-1}.[87]

A novel gold nanoparticles-poly(propylene imine) dendrimer- based platform was developed for the impedimetric detection of AFP.[88] The immunosensor thus prepared was used to detect AFP over a wide concentration range from 0.005 to 500 ng mL^{-1} with LOD of 0.00185 ng mL^{-1}.[88]

4.2. Carcinoembryonic Antigen

Carcinoembryonic antigen (CEA) is a highly glycosylated cell surface protein consisting of approx. 60% carbohydrates; its molecular mass is around 180–200 kDa.[89] The level of CEA in the serum of adult non-smokers is below 2.5 ng mL^{-1} and in the serum of smokers below 5.0 ng mL^{-1} and an elevated level of CEA is associated with lung cancer, breast cancer, colon cancer and cystadenocarcinoma.[90] Hence, the rapid and sensitive detection of low concentrations of CEA in serum could be the key to the early diagnosis of cancer and the further monitoring of the response of tumors to therapy. A large number of papers have been published detecting CEA in recent years, but only a few were based on EIS detection.

Fan with co-workers and Wang with his team prepared biosensors with linear ranges at the ng mL^{-1} concentration level, both using GCE modified with gold nanoparticles (AuNPs) with immobilized anti-CEA antibodies as a biorecognition element.[91,92] Another team sought to construct EIS biosensors employing staphylococcal protein A for the controlled immobilization of IgG with binding Fab fragments exposed to the electrolyte for binding their target antigens.[93] Staphylococcal protein A was immobilized onto AuNPs, which covered the surface of the gold electrode. Characterization of the biosensor revealed that EIS as well as cyclic voltammetry (CV) techniques can be employed for the determination of CEA, with EIS being the more sensitive. The biosensor exhibited LOD of 0.1 pg mL^{-1} with a good linear response to CEA in a range from 1 pg mL^{-1} to 100 ng mL^{-1}.[93]

The team of Professor Liu combined two methods: EIS and UV-Vis spectroscopy for sensitive CEA detection.[94] Their optoelectronic immunosensor was based on a gold-modified indium tin oxide (ITO) electrode and thiol-derivative-nanogold-(TDN)-labelled anti-CEA antibody. The linear range was observed between 0.05 and 80 ng mL^{-1} for EIS and 0.5 and 80 ng mL^{-1} for the UV method, respectively. EIS also exhibited a LOD (1 pg mL^{-1}) lower than the UV method (2 pg mL^{-1}).[94]

A higher sensitivity of the EIS immunosensor was achieved by using a combination of AuNPs with biocompatible polymeric nanoparticles γ-PGA-DA@CS, which were created by the self-assembling of chitosan (CS) and dopamine-modified poly(γ-glutamic acid) (γ-PGA-DA).[95] GCE was covered with γ-PGA-DA@CS in a process of electrophoretic deposition. Subsequently, AuNPs were anchored onto γ-PGA-DA@CS film and served as a highly stable and biocompatible immobilization platform for the attachment of monoclonal anti-CEA antibodies. The EIS response of the immunosensor changed linearly from 20 fg mL^{-1} to 20 ng mL^{-1} with very low LOD of 10 fg mL^{-1}.[95]

Because CEA is a cell surface protein, it is desirable to detect CEA-positive cells. There are two very important factors to be taken into account in the fabrication of an electrochemical cytosensor: electron transfer efficiency and biocompatibility. Jia with co-workers addressed these issues by using Au@BSA microspheres.[96] Au improved the electron transfer towards the electrode and bovine serum albumin (BSA) played a key role in achieving the biocompatibility. The Au@BSA microspheres thus prepared were applied on a gold electrode and were subsequently conjugated with anti-CEA antibodies *via* glutaraldehyde. Under optimal conditions, the final cytosensor exhibited a wide linear range from 5.2×10^{1} to 5.2×10^{7} cells mL^{-1} with LOD of 18 cells mL^{-1}.[96]

An alternative to antibodies as biorecognition elements are aptamers. The selective and sensitive detection of CEA was

achieved applying a platform based on (anti-CEA)/PBSE/Graphene/Cu-modified GCE by Srivastava and co-workers. The biosensor so developed exhibited a linear response in the physiological range of 1.0–25.0 ng mL^{-1} (normal value: ~5.0 ng mL^{-1}), revealing a sensitivity of 563 Ω ng^{-1} mL cm^{-2} with a correlation coefficient of 0.996 and LOD of 0.23 ng mL^{-1}.[97] In 2017, a specific aptasensor for the determination of CEA was constructed by Xu's team.[97] Their sensitive impedimetric aptasensor was based on a catalytic cascade for signal-amplification (Figure 6).

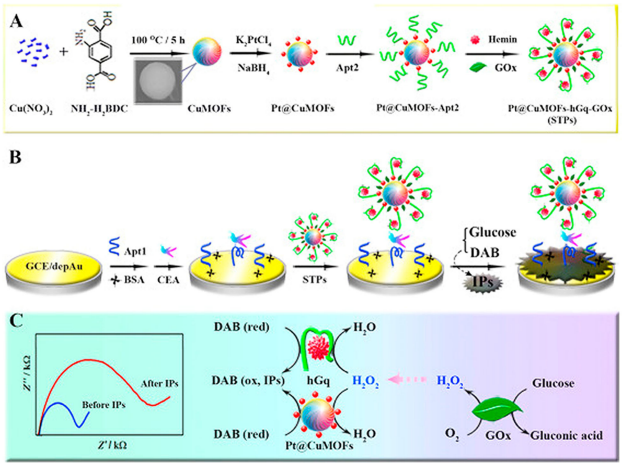

Figure 6. A) Preparation process of Pt@CuMOFs-hGq-GOx complex, B) Preparation of impedimetric aptasensor using Au-modified GCE electrode, aptamers, BSA as a blocking agent, and CEA as an analyte. Again, a sandwich configuration using the complex was used for CEA detection and glucose was used for hydrogen peroxide production using GOx and thus signal generation after a cascade reaction. C) Cascade catalysis amplification to form non-conductive insoluble precipitates (IPs), resulting in an increase in R_{CT} value. Reprinted from, [98] Copyright 2017, with permission from Elsevier.

The biosensing principle was based on the use of Cu-based metal organic frameworks (MOFs) coated with Pt nanoparticles (PtNPs) to obtain Pt@CuMOFs. After covering these particles with G-rich aptamer and hemin, the conformation of the CEA aptamer switched to hemin/G-quadruplex (hGq) (combination of iron-containing porphyrin and G-rich single-stranded DNA – mimicking a peroxidase-like activity). After adding glucose oxidase (GOx), they obtained Pt@CuMOFs-hGq-GOx, which acted as a signal transduction probe (STP). To detect CEA in samples, the CEA aptamer was immobilized on GCE with an electrodeposited Au layer. After incubation with CEA, a sandwich was formed by incubation with the STP and after the addition of glucose and dye, an insoluble precipitate was formed, which increased the impedimetric signal. The biosensor was able to detect CEA sensitively within a linear range from 0.05 pg mL^{-1} to 20 ng mL^{-1} with LOD of 0.023 pg mL^{-1}.[98]

Biomimetic materials are a relatively new type of biorecognition element in the construction of biosensors. Sales with coworkers constructed a CEA impedimetric sensor based on a "plastic antibody" assembled on an Ag-working electrode.[99] The advantage of this sensor was the low cost of the screen-printed Ag working electrodes prepared *via* printed-circuit board technology. The biomimetic material was prepared by the electropolymerization of pyrrole in the presence of CEA. After the formation of a polypyrrole matrix, CEA molecules were removed from the matrix by a proteolytic enzyme proteinase K creating a vacant site for the binding of CEA from the samples analyzed. The device exhibited a linear response from 0.05 to 1.25 pg mL^{-1} of CEA.[99] Finally, dye sensitized solar cells were fabricated with a counter electrode made of polypyrrole (PPy) that was made responsive to a specific protein by biomimetic material (BM) technology.[100] The resulting BM-PPy film acted as a biomimetic artificial antibody for CEA with LOD of 0.13 pg mL^{-1} [100]

4.3. Human Epidermal Growth Factor Receptors

The family of human epidermal growth factor receptors (HER/ErbB) includes four homologues: EGFR (HER1 or ErbB-1), HER2 (ErbB2), HER3 (ErbB3) and HER4 (ErbB4). These glycoproteins have a molecular mass ranging from 170 to 185 kDa and are localized in the cell membrane; they consist of an extracellular ligand-binding domain, a transmembrane part and an intracellular domain which possesses a tyrosine kinase activity.[101,102]

The chrono-impedance technique was applied to real-time monitoring of the interaction between HER3 and anti-HER3 as a biorecognition element.[102] The impedimetric biosensor based on self-assembled monolayers (SAMs) of 4-aminothiophenol on gold electrodes exhibited a linear response range from 0.4 to 2.4 pg mL^{-1} with LOD of 0.28 pg mL^{-1} (Figure 7).[102] The extracellular domain of these proteins serves as a binding site for ligands such as epidermal or transforming growth factors. After the attachment of a relevant ligand, tyrosine kinase activity in the intracellular domain is promoted, causing cell differentiation and proliferation.[103] Even though there is no known ligand which binds to HER2, the protein can be activated by the formation of heterodimers with other members of HER family receptors. For example, the HER2/HER3 dimer is the most potent oncogenic pair. During the formation of this dimer, kinase activity is switched on followed by the activation of downstream signaling pathways. The over-expression of mem-

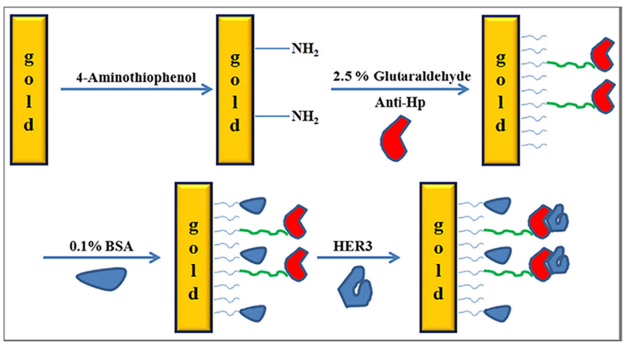

Figure 7. Schematic representation of immobilisation steps of anti-HER3 onto Au electrode. Reprinted from,[102] Copyright 2014, with permission from Elsevier.

bers of HER/ErbB family is hence associated with various types of cancer.[104,105] EGFR (HER1/ErbB1) was the first known growth factor receptor from HER family related to oncoproteins.[106] Its over-expression is associated with various tumors (non-small cell lung cancer, breast, ovarian, prostate, pancreatic, renal, head and neck, colorectal cancer, *etc.*) and also with a poor prognosis and development of aggressive disease stages.[107]

Zoroub with co-workers manufactured an EIS immunosensor for the sensitive determination of EGFR in samples.[108] The core of the biosensor consists of a polycrystalline Au electrode covered with AuNPs, an amine-terminated self-assembled monolayer (formed from cysteamine), a 1,4-phenylene diisothiocyanate linker and protein G applied to the controlled immobilization of antibodies. The biosensor exhibited a linear response from 1 pg mL^{-1} to 1 μg mL^{-1} with LOD of 0.34 pg mL^{-1}.[108] HER2 (ErbB2) is one of the best characterized and most widely used biomarkers. Physiological levels of HER2 in the blood of healthy people range from 4 to 14 ng mL^{-1}, while its concentration in the blood of cancer patients is higher (14–75 ng mL^{-1}). HER2 is over-expressed in around 20–30% of breast cancer patients and is also associated with an aggressive form of the disease and a poor prognosis.[109,110] Higher levels of HER2 were also observed during gastric, oesophageal, ovarian and endometrial cancers. Currently, there are two standardized methods for HER2 analysis (immunochemistry and *in-situ* fluorescence hybridization), but approximately 20% of assays are not accurate.[111]

Professor Lee with his team used a single-stranded DNA aptamer for the development of a biosensor.[112] Gold electrodes were covered with AuNPs and subsequently modified by 3-mercaptopropionic acid to produce SAM. A specific DNA aptamer was terminated with the amine group to form a covalent linkage with 3-mercaptopropionic acid. The biosensor exhibited good selectivity and sensitivity, and was able to detect the HER2 analyte in a linear fashion from 10^{-5} to 10^{2} ng mL^{-1}. A great advantage of this aptasensor was its simple regeneration by a pH-shift method, whereby a regenerated sensor worked as efficiently as a freshly prepared one.[112]

Marrazza's group used an affibody as a biorecognition element for the design of a label-free HER2 biosensor.[113] Affibodies are affinity proteins with low molecular mass (6.5 kDa), produced by protein engineering of one of the five stable α-helix bundle domains from IgG Fc-binding fragment of protein A from *Staphylococcus sp.*[114,115] Marrazza's affibodies were terminated with cysteine for better immobilization on the biosensor interface, which was formed by the deposition of nanostructured gold on graphite SPE modified with AuNPs and covered with 6-mercapto-1-hexanol to form SAM. Under optimal conditions, the affisensor could detect the human epidermal growth factor receptor 2 with LOD of 6.0 μg mL^{-1} within a linear range from 0 to 40 μg mL^{-1}.[113]

A thiol-terminated DNA aptamer with an affinity towards HER2 was used to prepare the bio-recognition layer *via* self-assembly on interdigitated gold surfaces.[109] Non-Faradaic EIS measurements were used as a detection scheme by detecting changes in capacitance. The aptasensor exhibited a linear range for the determination of HER2 from 1 pM to 100 nM in both a buffer and in undiluted serum with LOD below 1 pM.[109]

HER3 (ErbB3) was identified thanks to its homology to EGFR, but it was noted that the protein is the only member of the HER family which has impaired kinase activity. Normal levels of HER3 in a healthy person lie within 0.06 to 2.55 ng mL^{-1} and its over-expression (level increased up to 12 ng mL^{-1}) is associated with carcinomas of the breast, lung, oral cavity, ovarian, prostate, colon, pancreas and stomach.[116]

A novel Affimer-functionalized interdigitated electrode-based capacitive biosensor platform was developed for the detection and estimation of Her4 in undiluted serum.[117] The Affimer sensor exhibits high assay sensitivity with a wide dynamic range (from 1 pM to 100 nM) and LOD lower than 1 pM in both a buffer and in serum.[117]

We showed very recently, that also glycoprofiling of HER2 receptor in human sera might be a promising disease biomarker in the future (even though HER2 negative breast cancer patients without any serological HER2 are fairly common).[118] A disposable biosensor based on screen printed carbon electrodes with a deposited photoimmobilizable zwitterionic hydrogel layer was applied for covalent attachment of antibodies for a specific interaction with HER2 and subsequently for successful *in-situ* glycoprofiling of HER2 molecules using lectins. The EIS immunosensor detected HER2 down to 5 pg mL^{-1} (≈77 fM) with a minimal non-specific protein adsorption.[118]

A novel and potentially promising area emerged recently – assay of exosomes and microvesicules.[119] Nanoscale extracellular vesicles (EVs) including exosomes (membrane particles with size 50–150 nm) appeared as promising cancer biomarkers since they carry genetic information about the parental cells. Label-free EIS sensor measuring EVs secretion levels from hypoxic and normoxic MCF-7 cells (a breast cancer cell line) exhibited linear range from 10^{2} to 10^{9} EVs mL^{-1} with LOD of 77 EVs mL^{-1}.[119]

4.4. Carbohydrate Antigen 125, Carbohydrate Antigen 15.3, and Human Epididymis Protein 4

Carbohydrate antigen 125 (CA-125), also known as mucin 16 (MUC16), is a member of the mucin glycoproteins which contains 22,000 amino acids. It is significantly expressed by most ovarian epithelial tumors, but also by the normal epithelium of the female reproductive system, gastrointestinal mucosal cells, and by the luminal surface of the mesothelium lining the peritoneum, pleura and pericardium.[120]

The micro-flow label-free impedimetric biosensor was developed for the detection of CA125.[121] The immunosensor was based on the use of thin-film interdigitated gold-array microelectrodes (IDA). A good analytical performance for CA125 detection (from 0 to 100 U mL^{-1}) was achieved through the electropolymerization of anthranilic acid on IDA electrodes followed by the covalent attachment of the anti-CA125 monoclonal antibody. The estimated LOD ($3S_{blank}$/Slope) for CA125 was 7 U mL^{-1}.[121]

Carbohydrate antigen 15.3 (CA 15.3) was detected applying the immunoelectrode (anti-CA 15.3/SnO_2/Pt/Ti/glass).[122] The impedimetric biosensor (anti-CA 15.3/SnO_2/Pt/Ti/glass) exhibited a linear increase in the response upon incubation with CA 15–3, across a wide range of antigen concentrations from 50 ng dL^{-1} to 700 ng dL^{-1} (8 U mL^{-1} to 120 U mL^{-1}) with biosensor sensitivity of 38.6 Ω (ng dL^{-1})$^{-1}$, fast response time and a long shelf-life of more than 20 weeks.[122]

The human epididymis protein 4 (HE4) is a biomarker approved by the FDA for monitoring patients with epithelial ovarian cancer. The typical molecular mass of the protein is ~13 kDa for a single 50 amino acid non-glycosylated peptide HE4 molecule, classified as a whey acidic four-disulphide core protein.

HE4 is encoded by the WFDC2 gene located on chromosome 20q12-13.1 and belongs to the family of whey-acidic four-disulphide core proteins with suspected trypsin-inhibitor properties. HE4 is upregulated in ovarian cancer compared to other types of carcinomas and benign ovarian tumors.[123,124] The interdigitated electrode arrays with nano-scale gaps have been also successfully applied as a platform to the label-free detection of HE4.[124] The biomarker of ovarian cancer HE4 was detected along with CA-125 and CEA, which are well-established ovarian cancer biomarkers (Figure 8). The label-free impedimetric sensor successfully detected HE4 down to 1.5 ng mL^{-1} and this electronic sensor was able to differentiate all three biomarkers present in the same sample down to 100 pg mL^{-1}.[124]

4.5. Prostate Specific Antigen and p53 Protein

Prostate cancer (PCa, adenocarcinoma or glandular cancer of the prostate gland) represents the second commonest cancer in men worldwide, with an estimated 1.1 million cases diagnosed in 2012 alone. The prostate-specific antigen (PSA) belongs to the tissue kallikrein-related family of peptidases and is also known as γ-seminoprotein, kallikrein-3 or KLK3. PSA is a 28.4 kDa glycoprotein containing approximately 8% (by mass) of *N*-glycan with a single glycosylation site.

EIS was successfully applied as a label-free and non-destructive method to detection of the PSA cancer biomarker with low LODs.[125,126] The impedimetric biosensor based on recombinant single-chain antibody fragments (scAb), fragments covalently immobilized on the gold electrode surface, patterned by a mixed SAM using standard amine-coupling chemistry was developed.[125] The non-specific protein-binding was investigated applying a kallikrein 2 protein (a protein structurally similar to PSA) and the results indicated a high selectivity for PSA detection.[125] The impedimetric biosensor device was able to detect PSA down to 100 ag mL^{-1} with a linear concentration working range from 100 ag mL^{-1} up to 1 mg mL^{-1} (Figure 9).[127]

PSA analysis using a label-free PSA aptasensor and PSA immunosensor was based on graphene quantum dots-gold nanorods (GQDs-AuNRs) modified screen-printed electrodes.[128] Two modes of operation i.e., voltammetric and EIS techniques

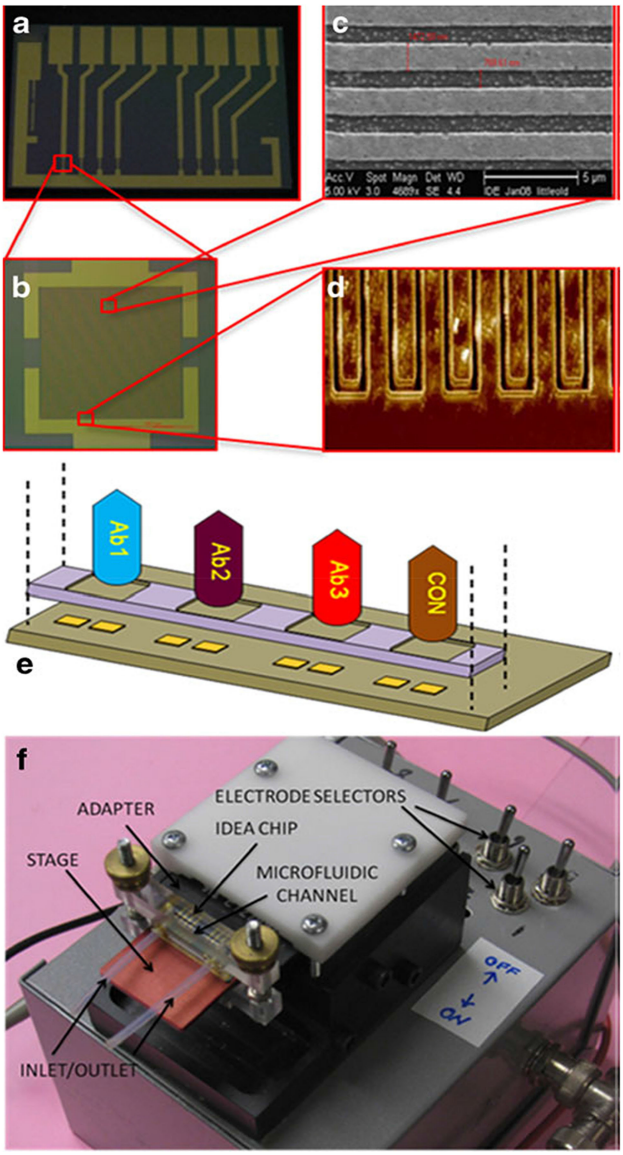

Figure 8. a) The nanogap IDEA chip with an array of eight IDEAs designed with contact electrodes in a SD card format. b) Photomicrograph of an individual IDE with 39 digits from each end. c) and d) SEM and AFM profiles of the IDEAs, e) shows the immobilisation process for multiplexed biosensor using physical segregation of electrodes using a PDMS mask. The chip was an integral part of the measurement set-up and microfluidics within a PDMS channel (f). Reprinted by permission from Springer,[124] COPYRIGHT (2012).

exhibited significant potential for reliable detection of the disease. Both sensors detected PSA with an almost same LOD of 0.14 ng mL^{-1}.[128]

Besides the detection of PSA, the EIS-based biosensor also made it possible to glycoprofile PSA using lectins on the same interface.[36] PSA could be detected down to 4 aM and the same ultralow PSA concentration could be applied to PSA glycoprofiling.[36]

A label-free immunosensor based on a tetra-armed star-shaped poly(glycidylmethacrylate)-modified disposable ITO electrode was fabricated for the detection of p53 protein, an important colorectal cancer biomarker.[129] The disposable im-

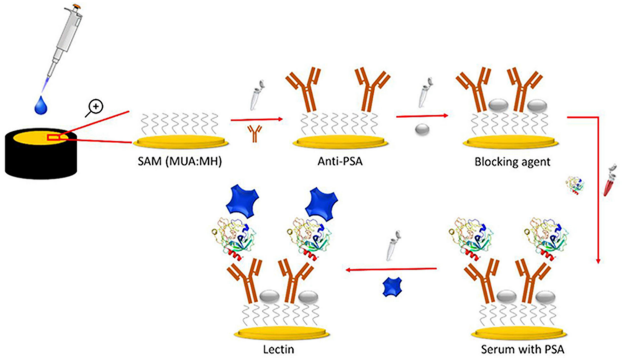

Figure 9. Construction of the biosensor device showing sensing of PSA and glycoprofiling of PSA by application of lectin. Reprinted from,[127] Copyright 2016, with permission from Elsevier.

munosensor exhibited LOD of 7 fg mL^{-1} and a linear detection range between 0.02 pg mL^{-1} and 4 pg mL^{-1}.[129]

A label-free immunosensor based on a tetra-armed star-shaped poly(glycidylmethacrylate)-modified disposable ITO electrode was fabricated for the detection of p53 protein, an important colorectal cancer biomarker.[129] The disposable immunosensor exhibited LOD of 7 fg mL^{-1} and a linear detection range between 0.02 pg mL^{-1} and 4 pg mL^{-1}.[129]

5. Challenges and Obstacles to Commercialization

For any potential application in clinical practice, the device needs to be able to perform robustly in a real sample without any further steps being required to provide a rapid method, and with a minute sample consumption. To enhance the performance of affinity biosensors, nanostructured interfaces are often prepared to increase the amount of probe immobilized on the surface.[130,131]

Increased interfacial density of the ligand can extend the linear range of the biosensor; however, if the probe density is too high, the biorecognition event can be suppressed due to steric hindrance.[45,135] This phenomenon varies from case to case, depending on the size and shape of the probe and the analyte, hence each device needs to be optimized and calibrated individually. For calibration of the device, positive and negative controls are often needed on the same surface, thus an array format of analysis is required,[136] reducing the input costs, increasing assay throughput and assay reliability. Mass production would also lead to the surfaces being produced in a reproducible way, as referred to in papers published to date. Sensitivity of detection is another very important issue since the biosensors need to detect low abundant cancer biomarkers with levels down to sub-ng mL^{-1} (Table 2).

Some of the highly abundant proteins in human serum may significantly interfere with analyte detection, lowering assay selectivity. It is, however, possible to reduce non-specific adsorption to a minimal level using surface modifications by different functionalities. For this purpose, molecules able to strongly bind and orient water molecules are applied to create a barrier against any non-specific interactions. Such surfaces highly resistant towards non-specific protein/cell binding are of interest not only for biomedical purposes (catheters and medical implants) but also to the food industry and to marine coatings.[137–143] Different molecules have been used to date, (especially in the form of hydrogels or SAMs),[139–141] mostly based on oligo(ethyleneglycol) (OEG) moieties or betaine derivatives.[41,142,144] In particular, zwitterionic betaine-based molecules are used to prepare 3D hydrogel layers, which are most effective in resisting non-specific protein-binding.[145]

Finally, for more user-friendly applications, analysis of other body fluids (not just serum samples) might be of a great importance in the field of impedimetric biosensing. For

Table 2. Brief overview of some recently published impedimetric biosensors for relevant cancer biomarkers detection.

BM	Cancer	Sensor	LR	LOD	Reg.	Ref
AFP	HpCa	GCE/CNH	0.001–60 ng mL^{-1}	0.33 pg mL^{-1}	–	[87]
CA125	OvCa	Au/#1	0–0.1 U mL^{-1}	0.0016 U mL^{-1}	A	[132]
CEA	CCa, PaCa, GaCa, BCa	GCE//#2	20 fg–20 ng mL^{-1}	10 fg mL^{-1}		[95]
HER2	BCa	GSPE/AuNP	0–40 μg L^{-1}	6.0 μg L^{-1}	B	[113]
HER2	BCa	Au/AuNP	10^{-5}–10^{2} ng mL^{-1}	5 ng mL^{-1}	C	[112]
HER2, HER4	BCa	IDμEs	1 pM–100 nM	1 pmol L^{-1}		[109]
HE4	OvCa	IDEA	1.5–25 ng mL^{-1}	1.5 ng mL^{-1}	–	[121]
FR_HeLa	CCT	BDD/AuNP	10–10^{5} cells mL^{-1}	10 cells mL^{-1}	D	[133]
PSA	PCa	Au	100 ag-1 mg mL^{-1}	100 ag mL^{-1}	-	[127]
RACK1	*	ITO	14–713 fg mL^{-1}	30 fg mL^{-1}	E	[134]

Abbreviations: BM: biomarkers; AFP: α-fetoprotein; GCE: glassy carbon electrode; SNH: single-walled carbon nanohorns; CA125: carbohydrate antigen 125; Au: gold electrode; #1: silica-coated gold nanoparticles; CEA: carcinoembryonic antigen; #2: gold nanoparticles and polymeric self-assembled nanoparticles (γ-PGA-DA@CS: chitosan and dopamine modified poly(γ-glutamic acid); HER2: human epidermal growth factor receptor 2; AuNP: gold nanoparticles; GSPE: gold nanostructured screen-printed graphite; IDμEs: interdigitated gold micro-electrode arrays on silicon/silicon oxide wafers"; HE4: human epididymis protein 4; IDEA: nanogap interdigitated electrode array (gold electrodes); FR_HeLa: folate receptor-rich human cervical carcinoma cells; BDD: boron-doped diamond electrode; PSA: prostate-specific antigen; RACK1: Receptor for Activated C Kinase 1; HpCa: hepatocellular cancer; GaCa: gastric cancer; CCT: cancerous cervical tumour; PCa: prostate cancer; ITO: indium tin oxide electrode; LR: linear range; * different types of cancer: oral squamous cell carcinoma, melanoma, colon cancer, on-small cell lung cancer, hepatocellular carcinoma and breast cancer; Reg: regeneration conditions; A: 0.15 M glycine-HCl, pH 2.0); B: 2 M HCl; C: PBS pH 4.0; D: 0.1 M citric acid/glycine/HCl, pH 3.0; E: 0.1 % HCl.

example analysis of interleukin 1β in a human saliva was performed.[146] An impedimetric immunosensor detected the analyte using a semi-conductive poly(2-thiophen-3-yl-malonic acid) (P3-TMA) layer as an immobilization matrix material and anti-IL-1β antibody as a biorecognition element. The relative change in impedance was proportional to the IL-1β concentration in the range from 0.01 to 3 pg mL^{-1} with LOD 3 fg mL^{-1}.[146]

6. Conclusions

This review details the theory of interfacial processes on the electrode surface and in close proximity to the conductive interface, which can significantly influence the electrochemical behaviour of the system. As a result, deviation from simple Nyquist plots could be observed, which can further complicate the evaluation of EIS assays. The article also describes what is required of EIS-based assays for successful integration into a device which could be applied in clinical practice or to design domestic devices. Finally, EIS-based assays protocols for the detection of cancer-associated biomarkers are described with details provided of the basic performance characteristics of these affinity-based biosensor devices. The article also discusses the need to address the non-specific binding of components from complex samples to design selective EIS-based biosensors.

So far especially antibody-based EIS biosensors have been constructed. It can be envisioned that biorecognition elements smaller than antibodies such as antibody fragments, DNA/RNA aptamers and peptide aptamers might in the future improve operational characteristics of affinity impedimetric biosensors such as enhanced operational/storage stability, sensitivity, specificity, assay reproducibility, robustness of a bioconjugation process and resistance towards non-specific binding from complex samples.

Acknowledgements

The financial support received from the Slovak Scientific Grant Agency VEGA 2/0137/18 and 2/0090/16 and the Slovak Research and Development Agency APVV 17-0300 and APW-15-0227 is acknowledged. The research received funding from the European Research Council (no. 311532). This publication is the result of the project implementation: Centre for materials, layers and systems for applications and chemical processes under extreme conditions – Stage I, ITMS No.: 26240120007, supported by the ERDF.

Conflict of Interest

The authors declare no conflict of interest.

Keywords: Biosensor · cancer · clinical diagnostics · electrochemical impedance spectroscopy · oncomarkers

[1] J. Barton, M. B. G. Garcia, D. H. Santos, P. Fanjul-Bolado, A. Ribotti, M. McCaul, D. Diamond, P. Magni, *Microchim. Acta* **2016**, *183*, 503–517.
[2] G. Buelbuel, A. Hayat, S. Andreescu, *Sensors* **2015**, *15*, 30736–30758.
[3] B. Martin-Fernandez, C. L. Manzanares-Palenzuela, M. Sanchez-Paniagua Lopez, N. de-los-Santos-Alvarez, B. Lopez-Ruiz, *Crit. Rev. Food Sci. Nutr.* **2017**, *57*, 2758–2774.
[4] W. Londeree, K. Davis, D. Helman, J. Abadie, *Havaii J. Med. Public Health* **2014**, *73*, 3–8.
[5] https://www.pointofcare.abbott/int/en/offerings/istat/istat-handheld.
[6] https://www.pointofcare.abbott/us/en/offerings/piccolo-xpress-chemistry-analyzer.
[7] J. D. Newman, A. P. F. Turner, *Biosens. Bioelectron.* **2005**, *20*, 2435–2453.
[8] J. Wang, *Chem. Rev.* **2008**, *108*, 814–825.
[9] J. Kim, A. S. Campbell, J. Wang, *Talanta* **2018**, *177*, 163–170.
[10] N. J. Forrow, G. S. Sanghera, S. J. Walters, J. L. Watkin, *Biosens. Bioelectron.* **2005**, *20*, 1617–1625.
[11] G. Rocchitta, A. Spanu, S. Babudieri, G. Latte, G. Madeddu, G. Galleri, S. Nuvoli, P. Bagella, M. I. Demartis, V. Fiore, R. Manetti, P. A. Serra, *Sensors* **2016**, *16*, 780.
[12] X. Luo, J. J. Davis, *Chem. Soc. Rev.* **2013**, *42*, 5944–5962.
[13] F. S. Felix, L. Angnes, *Biosens. Bioelectron.* **2018**, *102*, 470–478.
[14] Z. Tang, Z. Ma, *Biosens. Bioelectron.* **2017**, *98*, 100–112.
[15] E. Paleček, J. Tkáč, M. Bartošík, T. Bertók, V. Ostatná, J. Paleček, *Chem. Rev.* **2015**, *115*, 2045–2108.
[16] J. D. Cohen, L. Li, Y. Wang, C. Thoburn, B. Afsari, L. Danilova, C. Douville, A. A. Javed, F. Wong, A. Mattox, R. H. Hruban, C. L. Wolfgang, M. G. Goggins, M. Dal Molin, T. L. Wang, R. Roden, A. P. Klein, J. Ptak, L. Dobbyn, J. Schaefer, N. Silliman, M. Popoli, J. T. Vogelstein, J. D. Browne, R. E. Schoen, R. E. Brand, J. Tie, P. Gibbs, H. L. Wong, A. S. Mansfield, J. Jen, S. M. Hanash, M. Falconi, P. J. Allen, S. Zhou, C. Bettegowda, L. A. Diaz, Jr., C. Tomasetti, K. W. Kinzler, B. Vogelstein, A. M. Lennon, N. Papadopoulos, *Science* **2018**, *359*, 926–930.
[17] D. Xu, X. Huang, J. Guo, X. Ma, *Biosens. Bioelectron.* **2018**, *110*, 78–88.
[18] G. Maduraiveeran, M. Sasidharan, V. Ganesan, *Biosens. Bioelectron.* **2018**, *103*, 113–129.
[19] E. T. S. G. da Silva, D. E. P. Souto, J. T. C. Barragan, J. d. F. Giarola, A. C. M. de Moraes, L. T. Kubota, *ChemElectroChem* **2017**, *4*, 778–794.
[20] https://www.gminsights.com/industry-analysis/biosensors-market.
[21] https://globenewswire.com/news-release/2016/09/01/868793/0/en/Biosensors-Market-size-set-to-exceed-29bn-by-2024-Global-Market-Insights-Inc.html.
[22] E. B. Bahadır, M. K. Sezgintürk, *Artif. Cells, Nanomed., Biotechnol.* **2016**, *44*, 248–262.
[23] H. Li, X. Liu, L. Li, X. Mu, R. Genov, A. Mason, *Sensors* **2017**, *17*, 74.
[24] A. Wisitsoraat, J. P. Mensing, C. Karuwan, C. Sriprachuabwong, K. Jaruwongrungsee, D. Phokharatkul, T. M. Daniels, C. Liewhiran, A. Tuantranont, *Biosens. Bioelectron.* **2017**, *87*, 7–17.
[25] http://www.dropsens.com/en/screen_printed_electrodes_pag.html.
[26] Z. V. Živcová, V. Petrák, O. Frank, L. Kavan, *Diamond Relat. Mater.* **2015**, *55*, 70–76.
[27] A. Michalska, A. Kisiel, K. Maksymiuk in *Screen-Printed Disposable Reference Electrodes, Vol.* (Eds.: G. Inzelt, A. Lewenstam, F. Scholz), Springer Berlin Heidelberg, Berlin, Heidelberg, **2013**, pp.325–330.
[28] M. W. Shinwari, D. Zhitomirsky, I. A. Deen, P. R. Selvaganapathy, M. J. Deen, D. Landheer, *Sensors* **2010**, *10*, 1679–1715.
[29] I. Palchetti, *Bioanalysis* **2014**, *6*, 3417–3435.
[30] S. Campuzano, P. Yáñez-Sedeño, J. M. Pingarrón, *Curr. Opin. Electrochem.* **2018**, DOI: 10.1016/j.coelec.2018.04.015.
[31] E. Palecek, M. Bartosik, *Chem. Rev.* **2012**, *112*, 3427–3481.
[32] E. Katz, I. Willner, *Electroanalysis* **2003**, *15*, 913–947.
[33] J. R. Macdonald, *Ann. Biomed. Eng.* **1992**, *20*, 289–305.
[34] J. R. Macdonald, *Electrochim. Acta* **1990**, *35*, 1483–1492.
[35] J. S. Daniels, N. Pourmand, *Electroanalysis* **2007**, *19*, 1239–1257.
[36] D. Pihikova, S. Belicky, P. Kasak, T. Bertok, J. Tkac, *Analyst* **2016**, *141*, 1044–1051.
[37] S. Vogt, Q. Su, C. Gutiérrez-Sánchez, G. Nöll, *Anal. Chem.* **2016**, *88*, 4383–4390.
[38] L. Kluková, T. Bertok, P. Kasák, J. Tkac, *Anal. Methods* **2014**, *6*, 4922–4931.
[39] J. C. Love, L. A. Estroff, J. K. Kriebel, R. G. Nuzzo, G. M. Whitesides, *Chem. Rev.* **2005**, *105*, 1103–1170.
[40] J. E. B. Randles, *Discuss. Faraday Soc.* **1947**, *1*, 11–19.
[41] A. Hushegyi, T. Bertok, P. Damborsky, J. Katrlik, J. Tkac, *Chem. Commun.* **2015**, *51*, 7474–7477.

[42] T. Bertok, L. Klukova, A. Sediva, P. Kasák, V. Semak, M. Micusik, M. Omastova, L. Chovanová, M. Vlček, R. Imrich, A. Vikartovska, J. Tkac, *Anal. Chem.* **2013**, *85*, 7324–7332.
[43] L. Klukova, T. Bertok, M. Petrikova, A. Sediva, D. Mislovicova, J. Katrlik, A. Vikartovska, J. Filip, P. Kasak, A. Andicsová-Eckstein, J. Mosnáček, J. Lukáč, J. Rovenský, R. Imrich, J. Tkac, *Anal. Chim. Acta* **2015**, *853*, 555–562.
[44] T. Bertok, A. Sediva, J. Katrlik, P. Gemeiner, M. Mikula, M. Nosko, J. Tkac, *Talanta* **2013**, *108*, 11–18.
[45] T. Bertok, A. Sediva, A. Vikartovska, J. Tkac, *Int. J. Electrochem. Sci.* **2014**, *9*, 890–900.
[46] D. Damborska, T. Bertok, E. Dosekova, A. Holazova, L. Lorencova, P. Kasak, J. Tkac, *Microchim. Acta* **2017**, *184*, 3049–3067.
[47] C. Dariane, C. Le Cossec, S. J. Drouin, B. Wolff, B. Granger, P. Mozer, M.-O. Bitker, S. F. Shariat, O. Cussenot, M. Rouprêt, *World J. Urol.* **2014**, *32*, 481–487.
[48] http://www.ivium.nl/pocketstat.
[49] https://www.palmsens.com/product/palmsens4/.
[50] J. J. Giner-Sanz, E. M. Ortega, V. Pérez-Herranz, *Electrochim. Acta* **2016**, *209*, 254–268.
[51] R. Esfandyarpour, H. Esfandyarpour, M. Javanmard, J. S. Harris, R. W. Davis, *Sens. Actuat. B: Chem.* **2013**, *177*, 848–855.
[52] M. E. Orazem, P. Agarwal, L. H. Garcia-Rubio, *J. Electroanal. Chem.* **1994**, *378*, 51–62.
[53] Z. O. Uygun, H. D. Ertuğrul Uygun, *Sens. Actuat. B: Chem.* **2014**, *202*, 448–453.
[54] R. Ohno, H. Ohnuki, H. Wang, T. Yokoyama, H. Endo, D. Tsuya, M. Izumi, *Biosens. Bioelectron.* **2013**, *40*, 422–426.
[55] R. E. Ionescu, N. Jaffrezic-Renault, L. Bouffier, C. Gondran, S. Cosnier, D. G. Pinacho, M. P. Marco, F. J. Sánchez-Baeza, T. Healy, C. Martelet, *Biosens. Bioelectron.* **2007**, *23*, 549–555.
[56] T. Yang, S. Wang, H. Jin, W. Bao, S. Huang, J. Wang, *Sens. Actuat. B: Chem.* **2013**, *178*, 310–315.
[57] A. Ramanavicius, P. Genys, A. Ramanaviciene, *Electrochim. Acta* **2014**, *146*, 659–665.
[58] S. Chandra, N. Barola, D. Bahadur, *Chem. Commun.* **2011**, *47*, 11258–11260.
[59] P. Jolly, N. Formisano, J. Tkáč, P. Kasák, C. G. Frost, P. Estrela, *Sens. Actuat. B: Chem.* **2015**, *209*, 306–312.
[60] J. Lehr, F. C. B. Fernandes, P. R. Bueno, J. J. Davis, *Anal. Chem.* **2014**, *86*, 2559–2564.
[61] P. R. Bueno, G. T. Feliciano, J. J. Davis, *Phys. Chem. Chem. Phys.* **2015**, *17*, 9375–9382.
[62] M. Schönleber, D. Klotz, E. Ivers-Tiffée, *Electrochim. Acta* **2014**, *131*, 20–27.
[63] M. C. Rodriguez, A. N. Kawde, J. Wang, *Chem. Commun.* **2005**, 4267–4269.
[64] M. N. Sonuç, M. K. Sezgintürk, *Curr. Anal. Chem.* **2016**, *12*, 43–53.
[65] B. Ozcan, M. K. Sezginturk, *Talanta* **2016**, *160*, 367–374.
[66] V. F. Lvovich in *Impedance Instrumentation, Testing, and Data Validation, Vol.* John Wiley & Sons, Inc., **2012**, pp.163–204.
[67] E. K. Lenzi, J. L. de Paula, F. R. G. B. Silva, L. R. Evangelista, *J. Phys. Chem. C* **2013**, *117*, 23685–23690.
[68] W. Kucza, M. Danielewski, A. Lewenstam, *Electrochem. Commun.* **2006**, *8*, 416–420.
[69] B. Grysakowski, J. J. Jasielec, B. Wierzba, T. Sokalski, A. Lewenstam, M. Danielewski, *J. Electroanal. Chem.* **2011**, *662*, 143–149.
[70] S. E. Feicht, A. S. Khair, *Soft Matter* **2016**, *12*, 7028–7037.
[71] G. Barbero, A. L. Alexe-Ionescu, *Liq. Cryst.* **2005**, *32*, 943–949.
[72] G. Barbero, M. Scalerandi, *J. Chem. Phys.* **2012**, *136*, 084705.
[73] M. Z. Bazant, K. Thornton, A. Ajdari, *Phys. Rev. E* **2004**, *70*, 021506.
[74] Y. Xie, J. Li, C. Yuan, *Electrochim. Acta* **2014**, *127*, 266–275.
[75] S. E. Li, B. Wang, H. Peng, X. Hu, *J. Power Sources* **2014**, *258*, 9–18.
[76] A. A. Moya, *J. Phys. Chem. C* **2016**, *120*, 6543–6552.
[77] F. Pittino, L. Selmi, *Comput. Methods Appl. Mechan. Eng.* **2014**, *278*, 902–923.
[78] Y. Cha, M. Aureli, M. Porfiri, *J. Appl. Phys.* **2012**, *111*, 124901.
[79] F. Pittino, P. Scarbolo, F. Widdershoven, L. Selmi, *IEEE Trans. Nanotechnol.* **2015**, *14*, 709–716.
[80] F. Pittino, L. Selmi, F. Widdershoven, *Solid-State Electron.* **2013**, *88*, 82–88.
[81] N. Couniot, A. Afzalian, N. Van Overstraeten-Schlögel, L. A. Francis, D. Flandre, *Sens. Actuat. B: Chem.* **2015**, *211*, 428–438.
[82] A. J. Atkinson, Colburn, W. A. DeGruttola, V. G. DeMets, D. L. Downing, G. J. Hoth, D. F. Oates, J. A. Peck, C. C. Schooley, R. T. Spilker, B. A. Woodcock, J. Zeger, S. L. Zeger, *Clin. Pharmacol. Ther.* **2001**, *69*, 89–95.
[83] A. K. Füzéry, J. Levin, M. M. Chan, D. W. Chan, *Clin. Proteomics* **2013**, *10*, 13.
[84] A. Mordente, E. Meucci, G. E. Martorana, A. Silvestrini in *Cancer Biomarkers Discovery and Validation: State of the Art, Problems and Future Perspectives, Vol.* (Ed. R. Scatena), Springer Netherlands, Dordrecht, **2015**, pp.9–26.
[85] J. Liu, G. Lin, C. Xiao, Y. Xue, A. Yang, H. Ren, W. Lu, H. Zhao, X. Li, Z. Yuan, *Biosens. Bioelectron.* **2015**, *71*, 82–87.
[86] H. Yang, Z. Li, X. Wei, R. Huang, H. Qi, Q. Gao, C. Li, C. Zhang, *Talanta* **2013**, *111*, 62–68.
[87] F. Yang, J. Han, Y. Zhuo, Z. Yang, Y. Chai, R. Yuan, *Biosens. Bioelectron.* **2014**, *55*, 360–365.
[88] A. O. Idris, N. Mabuba, O. A. Arotiba, *Electroanalysis* **2018**, *30*, 31–37.
[89] S. Kumar, M. Willander, J. G. Sharma, B. D. Malhotra, *J. Mater. Chem. B* **2015**, *3*, 9305–9314.
[90] S. Kumar, M. Willander, J. G. Sharma, B. D. Malhotra, *J. Mater. Chem. B* **2015**, *3*, 9305–9314.
[91] Y. Li, Z. Zhang, Y. Zhang, D. Deng, L. Luo, B. Han, C. Fan, *Biosens. Bioelectron.* **2016**, *79*, 536–542.
[92] Y. Li, Y. Chen, D. Deng, L. Luo, H. He, Z. Wang, *Sens. Actuators B: Chem.* **2017**, *248*, 966–972.
[93] J. Zhou, L. Du, L. Zou, Y. Zou, N. Hu, P. Wang, *Sens. Actuators B: Chem.* **2014**, *197*, 220–227.
[94] H. Zeng, D. A. Y. Agyapong, C. Li, R. Zhao, H. Yang, C. Wu, Y. Jiang, Y. Liu, *Sens. Actuators B: Chem.* **2015**, *221*, 22–27.
[95] S. Xu, R. Zhang, W. Zhao, Y. Zhu, W. Wei, X. Liu, J. Luo, *Biosens. Bioelectron.* **2017**, *92*, 570–576.
[96] C. Hu, D.-P. Yang, Z. Wang, L. Yu, J. Zhang, N. Jia, *Anal. Chem.* **2013**, *85*, 5200–5206.
[97] V. K. Singh, S. Kumar, S. K. Pandey, S. Srivastava, M. Mishra, G. Gupta, B. D. Malhotra, R. S. Tiwari, A. Srivastava, *Biosens. Bioelectron.* **2018**, *105*, 173–181.
[98] X. Zhou, S. Guo, J. Gao, J. Zhao, S. Xue, W. Xu, *Biosens. Bioelectron.* **2017**, *98*, 83–90.
[99] F. T. Moreira, M. J. M. Ferreira, J. R. Puga, M. G. F. Sales, *Sens. Actuators B: Chem.* **2016**, *223*, 927–935.
[100] F. T. C. Moreira, L. A. A. N. A. Truta, M. G. F. Sales, *Sci. Rep.* **2018**, *8*.
[101] P. Seshacharyulu, M. P. Ponnusamy, D. Haridas, M. Jain, A. K. Ganti, S. K. Batra, *Expert Opin. Ther. Targets* **2012**, *16*, 15–31.
[102] M. N. Sonuç, M. K. Sezgintürk, *Talanta* **2014**, *120*, 355–361.
[103] G. Bethune, D. Bethune, N. Ridgway, Z. Xu, *J. Thorac. Dis.* **2010**, *2*, 48.
[104] S.-H. I. Ou, A. B. Schrock, E. V. Bocharov, S. J. Klempner, C. K. Haddad, G. Steinecker, M. Johnson, B. J. Gitlitz, J. Chung, P. V. Campregher, *J. Thorac. Oncol.* **2017**, *12*, 446–457.
[105] Y.-J. Kim, D. Sung, E. Oh, Y. Cho, T.-M. Cho, L. Farrand, J. H. Seo, J. Y. Kim, *Cancer Lett.* **2018**, *412*, 118–130.
[106] S. Maramotti, M. Paci, G. Manzotti, C. Rapicetta, M. Gugnoni, C. Galeone, A. Cesario, F. Lococo, *Int. J. Mol. Sci.* **2016**, *17*, 593.
[107] F. Tas, E. Bilgin, S. Karabulut, D. Duranyildiz, *Cytokine* **2015**, *71*, 66–70.
[108] R. Elshafey, A. C. Tavares, M. Siaj, M. Zourob, *Biosens. Bioelectron.* **2013**, *50*, 143–149.
[109] S. K. Arya, P. Zhurauski, P. Jolly, M. R. Batistuti, M. Mulato, P. Estrela, *Biosens. Bioelectron.* **2018**, *102*, 106–112.
[110] A. Sinibaldi, C. Sampaoli, N. Danz, P. Munzert, L. Sibilio, F. Sonntag, A. Occhicone, E. Falvo, E. Tremante, P. Giacomini, *Biosens. Bioelectron.* **2017**, *92*, 125–130.
[111] N. Iqbal, N. Iqbal, *Mol. Biol. Int.* **2014**, *2014*.
[112] L. Chun, S.-E. Kim, M. Cho, W.-s. Choe, J. Nam, D. W. Lee, Y. Lee, *Sens. Actuators B: Chem.* **2013**, *186*, 446–450.
[113] A. Ravalli, C. G. da Rocha, H. Yamanaka, G. Marrazza, *Bioelectrochemistry* **2015**, *106*, 268–275.
[114] J. Löfblom, J. Feldwisch, V. Tolmachev, J. Carlsson, S. Ståhl, F. Y. Frejd, *FEBS Lett.* **2010**, *584*, 2670–2680.
[115] F. Y. Frejd, K.-T. Kim, *Exp. Mol. Med.* **2017**, *49*, e306.
[116] K. Mujoo, B.-K. Choi, Z. Huang, N. Zhang, Z. An, *Oncotarget* **2014**, *5*, 10222–10236.
[117] P. Zhurauski, S. K. Arya, P. Jolly, C. Tiede, D. C. Tomlinson, P. K. Ferrigno, P. Estrela, *Biosens. Bioelectron.* **2018**, *108*, 1–8.
[118] E. Chocholova, T. Bertok, L. Lorencova, A. Holazova, P. Farkas, A. Vikartovska, V. Bella, D. Velicova, P. Kasak, A. A. Eckstein, J. Mosnacek, D. Hasko, J. Tkac, *Sens. Actuators B: Chem.* **2018**, *272*, 626–633.

[119] T. Kilic, A. T. D. S. Valinhas, I. Wall, P. Renaud, S. Carrara, *Sci. Rep.* **2018**, *80*.
[120] K. Al-Musalhi, M. Al-Kindi, F. Ramadhan, T. Al-Rawahi, K. Al-Hatali, W.-A. Mula-Abed, *Oman Med. J.* **2015**, *30*, 428.
[121] A. Ravalli, L. Lozzi, G. Marrazza, *Curr. Drug Delivery* **2016**, *13*, 400–408.
[122] K. Arora, M. Tomar, V. Gupta, *Anal. Methods* **2017**, *9*, 6549–6559.
[123] K. D. Steffensen, M. Waldstrøm, I. Brandslund, B. Lund, S. M. Sørensen, M. Petzold, A. Jakobsen, *Oncol. Lett.* **2016**, *11*, 3967–3974.
[124] A. M. Whited, K. V. Singh, D. Evans, R. Solanki, *BioNanoScience* **2012**, *2*, 161–170.
[125] S. Belicky, P. Damborsky, J. Zapatero-Rodríguez, R. O'Kennedy, J. Tkac, *Electrochim. Acta* **2017**, *246*, 399–405.
[126] D. Pihikova, Z. Pakanova, M. Nemcovic, P. Barath, S. Belicky, T. Bertok, P. Kasak, J. Mucha, J. Tkac, *Proteomics* **2016**, *16*, 3085–3095.
[127] D. Pihikova, P. Kasak, P. Kubanikova, R. Sokol, J. Tkac, *Anal. Chim. Acta* **2016**, *934*, 72–79.
[128] M. Srivastava, N. R. Nirala, S. K. Srivastava, R. Prakash, *Sci. Rep.* **2018**, *8*.
[129] M. Aydın, E. B. Aydın, M. K. Sezgintürk, *Biosens. Bioelectron.* **2018**, *107*, 1–9.
[130] E. Dosekova, J. Filip, T. Bertok, P. Both, P. Kasak, J. Tkac, *Med. Res. Rev.* **2017**, *37*, 514–626.
[131] M. Holzinger, A. Le Goff, S. Cosnier, *Front. Chem.* **2014**, *2*, 63.
[132] M. Johari-Ahar, M. Rashidi, J. Barar, M. Aghaie, D. Mohammadnejad, A. Ramazani, P. Karami, G. Coukos, Y. Omidi, *Nanoscale* **2015**, *7*, 3768–3779.
[133] J. Weng, Z. Zhang, L. Sun, J. A. Wang, *Biosens. Bioelectron.* **2011**, *26*, 1847–1852.
[134] E. B. Bahadr, M. K. Sezginturk, *Analyst* **2016**, *141*, 5618–5626.
[135] A. W. Peterson, R. J. Heaton, R. M. Georgiadis, *Nucleic Acids Res.* **2001**, *29*, 5163–5168.
[136] T. Bertok, E. Dosekova, S. Belicky, A. Holazova, L. Lorencova, D. Mislovicova, D. Paprckova, A. Vikartovska, R. Plicka, J. Krejci, M. Ilcikova, P. Kasak, J. Tkac, *Langmuir* **2016**, *32*, 7070–7078.
[137] V. B. Damodaran, N. S. Murthy, *Biomater. Res.* **2016**, *20*, 18.
[138] J. S. Rees, K. S. Lilley, *Methods* **2011**, *54*, 407–412.
[139] A. A. Beltran-Osuna, B. Cao, G. Cheng, S. C. Jana, M. P. Espe, B. Lama, *Langmuir* **2012**, *28*, 9700–9706.
[140] S. Jiang, Z. Cao, *Adv. Mater.* **2010**, *22*, 920–932.
[141] B. Cao, Q. Tang, G. Cheng, *J. Biomater. Sci. Polym. Ed.* **2014**, *25*, 1502–1513.
[142] M. A. Benvenuto, E. S. Roberts-Kirchhoff, M. N. Murray, D. M. Garshott, *It's All in the Water: Studies of Materials and Conditions in Fresh and Salt Water Bodies*, ACS Publications, **2011**.
[143] T. Bertok, A. Šedivá, J. Filip, M. Ilcikova, P. Kasak, D. Velic, E. Jane, M. Mravcová, J. Rovenský, P. Kunzo, P. Lobotka, V. Šmatko, A. Vikartovská, J. Tkac, *Langmuir* **2015**, *31*, 7148–7157.
[144] M. A. Benvenuto, E. S. Roberts-Kirchhoff, M. N. Murray, D. M. Garshott in *It's All in the Water: Studies of Materials and Conditions in Fresh and Salt Water Bodies*, Vol. 1086 (Ed. Eds.: Editor), American Chemical Society, City, **2011**, pp.0.
[145] H. Lisalova, E. Brynda, M. Houska, I. Visova, K. Mrkvova, X. C. Song, E. Gedeonova, F. Surman, T. Riedel, O. Pop-Georgievski, J. Homola, *Anal. Chem.* **2017**, *89*, 3524–3531.
[146] E. B. Aydın, M. Aydın, M. K. Sezgintürk, *Sens. Actuat. B: Chem.* **2018**, *270*, 18–27.

Manuscript received: June 22, 2018
Accepted manuscript online: September 1, 2018
Version of record online: September 21, 2018